On the competition between homogeneous and inhomogeneous broadening of orbital transitions in Si:Bi

N. Stavrias, K. Saeedi, and B. Redlich

Radboud University, Institute for Molecules and Materials,

FELIX Laboratory, Toernooiveld 7c,

6525 ED Nijmegen, The Netherlands

P.T. Greenland

London Centre for Nanotechnology and Department of Physics and Astronomy,

University College London, London WC1H 0AH, UK

H. Riemann, N.V. Abrosimov

Leibniz-Institut für Kristallzüchtung (IKZ), 12489 Berlin, Germany

M.L.W. Thewalt

Department of Physics, Simon Fraser University, Burnaby, BC V5A 1S6, Canada

C.R. Pidgeon

Institute of Photonics and Quantum Science, SUPA,

Heriot-Watt University, Edinburgh EH14 4AS

B.N. Murdin*

Advanced Technology Institute and SEPNet,

University of Surrey, Guildford, Surrey, GU2 7XH, UK

(Dated: September 11, 2017)

Abstract

We present results for the lifetime of the orbital transitions of Bi donors in Si, measured using both frequency domain and time-domain techniques, allowing us to distinguish between homogeneous and inhomogeneous processes. The proximity of the energy of the optically allowed transitions to the optical phonon energy means that there is an unusually wide variation in the lifetimes and broadening mechanisms for this impurity, from fully homogeneous lifetime-broadened transitions to fully inhomogeneously broadened lines. The relaxation lifetime (T_1) of the states range from the low 10's to 100's of ps, and we find that there is little extra dephasing (so that T_1 is of the order of $T_2/2$) in each case.

I. INTRODUCTION

Donors in silicon have been studied extensively due to their uses in silicon electronics. Since the proposal of silicon donor based quantum computing schemes[1] research has moved towards producing single donor based qubits[2]. Most effort has focused on the phosphorus donor, with the placement and spin readout of single donors recently demonstrated[3]. Although the record qubit memory storage times have been found for ^{31}P donors in bulk ^{28}Si[4,5], bismuth donors in silicon have a number of advantages for quantum information processing, due to having a large nuclear spin ($I_N = 9/2$) and large hyperfine coupling, providing e.g. "clock transitions" which are immune to field noise[6,7].

Orbital transitions are also important parts of the tool kit, with one qubit gating scheme utilizing them to provide the gating mechanism[8]. In the time domain, phosphorus is well studied with respect to orbital transitions, and pulsed experiments have revealed population relaxation times [9,10], dephasing times [11] and free-induction decay or Ramsey interference times [12]. Bismuth has gained further attention since its state might be prepared with an optical pumping scheme similar to that used for free alkali metal atoms[13].

While the excited states of all the Group V impurities have very similar binding energies, their ground states are affected by a chemical shift, which is particularly large in Si:Bi; the orbital transitions are thus at much shorter wavelength[14–16], in fact, just within range of quantum cascade lasers, which could therefore be used for optical pumping in Si:Bi. In order to understand the optical pumping process, it is important to study the relaxation dynamics.

Now, absorption spectroscopy provides valuable information on the linewidth, and in the case of homogeneous broadened lines this can be related to the dynamics. The line width is generally given by a convolution with inhomogeneous effects[17], although progress in sample preparation has allowed observation of homogeneous lines in Si:P and Si:B[18]. Where the lines are not clearly homogeneous, time-domain measurements must be used to extract the dynamics instead. The Si:Bi system is interesting because the $2p$ states are resonant with the optical phonons contrasting with higher excited states which have no direct phonon relaxation pathway. A range of dynamical processes are therefore available in a single system.

In this work we present measurements of the lifetime of the excited Bi donor orbitals us-

ing time domain pump-probe techniques with the free electron laser facility FELIX, which we then compare with a new analysis of previously published Fourier Transform Infra-Red (FTIR) spectroscopy[13] from which we extract the homogeneous components of the absorption lineshape. There are currently no reports of time-resolved (pump-probe) spectroscopy for Si:Bi in the literature.

II. BACKGROUND

The level spectrum of Group V donors in silicon is hydrogen-like[16,17,19]. It is complicated by the fact that the conduction band minima are near the X-point of the Brillouin Zone, and the effective mass is anisotropic, which lifts the degeneracy between the $p_\pm$ and the p_0 odd-parity excited states. The ground state is further affected by the species-specific chemical shift, also known as the central cell potential, which deepens and splits it into three components of different symmetry, $1s(A_1, E, T_2)$. The binding energy of the lowest energy component, $1s(A_1)$, is strongly species dependent: for Si:P it is 45.59 meV and for Si:Bi it is 70.98 meV[1617]. The binding energies of the $1s(E, T_2)$ components are $\sim$32 meV with a relatively small splitting and variation among the species of ~ 2 meV[20]. The odd parity states such as $2p_0$ are also split into A_1, E, T_2 components but the splitting and species variation are negligible. The optically allowed transition from $1s(A_1)$ is for example, to $2p_0(T_2)$. The energy levels are shown in Fig. 1.

In Si:Bi the transition energy from the ground state to the first odd-parity excited state, $2p_0$, is very nearly resonant with the transverse optical (TO) phonon energy, producing a very fast relaxation directly back to the ground state and a very wide homogeneously broadened absorption line[14,16]. Higher excited states, with transitions back to the ground state that are further from resonance with the TO phonon, are longer lived, and sharper. For these higher states, direct relaxation by a single TO phonon becomes forbidden, and a cascade process is required involving relaxation down the ladder of excited states. The energy of each of these steps is small (the binding energy of $2p_0$ is 11.5 meV, 2.8 THz) and can only involve acoustical phonons. The momentum of these phonons is small (maximum $\sim 0.3 \times 2\pi/a$) and it is likely that they produce dominantly intravalley transitions, though at the highest energy they could also produce intervalley g-phonon transitions. There are limited calculations on the phonon relaxation rates.

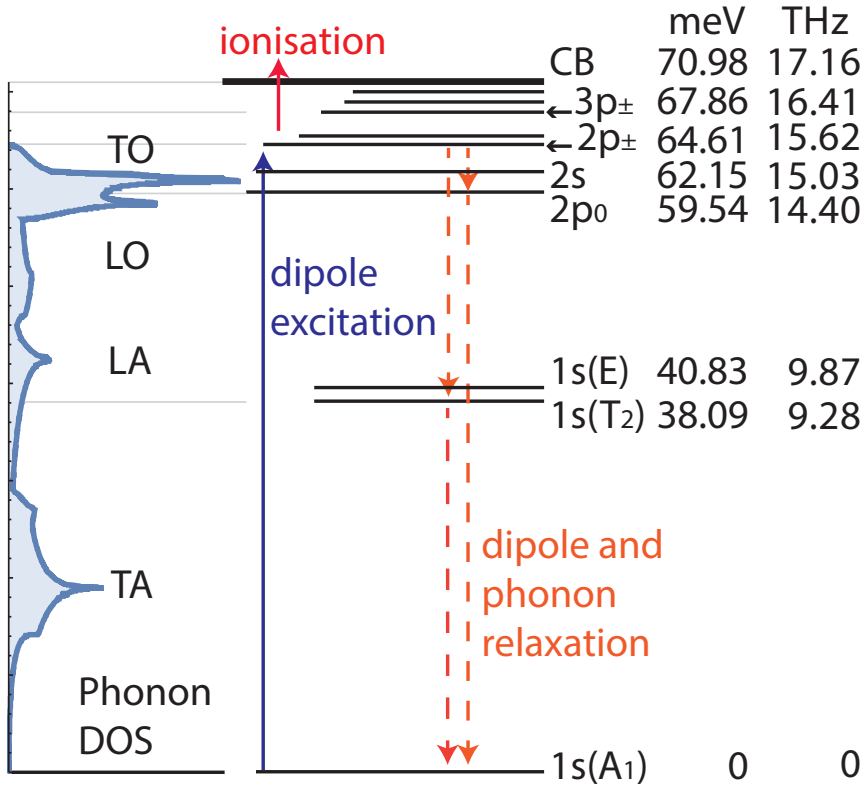

FIG. 1: Energy level diagram of Bi donors in Si, values from Refs[14–16,20]. The left hand side shows the phonon density of states (DOS) from Ref.[21] and indicates the position of the transverse optical (TO), longitudinal optical (LO), transverse acoustic (TA) and longitudinal acoustic phonons. The scale on the right hand side is the energy difference between the ground state and the excited orbital states.

The phonon matrix element is small when there are no large Fourier components of the product of the initial and final wavefunctions at $q = \Delta E/\hbar v$ where ΔE is the energy difference between the states and v is the sound velocity. Values for emission rates of intravalley phonons between pairs of the excited states $2p_0$, $2s$, $2p_\pm$, $3p_0$ and $3p_\pm$ have been given by Ref.[22]. In the case of the $2p_0$, $2s$, $2p_\pm$ and $3p_0$ all possible downward transition rates among the four states are given, and the fastest rate in each case is for emission of an intravalley LA phonon to the $2p_0$. The lifetimes for intravalley LA phonons for $2p_\pm \rightarrow 2p_0$ and $3p_0 \rightarrow 2p_0$ relaxation are 70 ps and 40 ps respectively, while emission of lower energy phonons e.g. from $3p_0 \rightarrow 2s$ etc or emission of TA phonons is much slower. For $3p_\pm$, only rates for relaxation to $3p_0$ and $2p_\pm$ were given by Ref.[22], not $3p_\pm \rightarrow 2p_0$, which may well be dominant since relaxation to $2p_0$ dominates the $2p_\pm$ and the $3p_0$. These intervalley transition

rates between excited states are presumably independent of species. Intravalley acoustical phonon relaxation lifetimes from the excited states to the $1s$ state are also given[22], but excluding the effects of the central cell correction. There is no calculation of the relaxation from the excited states to the $1s(E, T_2)$ via intervalley or intravalley phonons including the central cell correction other than for $2p_0$ and the $1s(E)$ and $1s(T_2)$[22], but these acoustical phonon rates are presumed to be irrelevant in the case of Si:Bi where $2p_0 \rightarrow 1s(A_1)$ by optical phonon emission is very fast. It seems reasonable to expect that the trends should continue, which would predict that for Si:Bi the relaxation is by either direct relaxation with an optical phonon (for the lowest states) or by a two-step cascade relaxation from the excited state to the $2p_0$ by LA phonon emission followed by optical phonon emission back to the ground state. It is worth noting here that as in Bi, the higher lying states in the more shallow P and B impurities in ^{28}Si sharpen with increasing state number[18]. Trends are rather difficult to identify, but evidently the matrix element drops as the quantum number rises, but not in a simple monotonic way. More theory is required to understand the relaxation mechanisms from the higher states.

Population inversion and lasing from the $2p_\pm$ to $1s(E, T_2)$ states in Si:Bi pumped with a CO_2 laser, but not from $2p_0$ or $2s$ is consistent with the model of fast phonon mediated relaxation from the $2p_0$ and $2s$ states and much slower relaxation from the higher states[23].

There are a number of sources of inhomogeneity that affect the spectroscopy. Concentration broadening of the excited state causes a rather sudden rise in the inhomogeneous broadening when excited states begin to overlap. At $1(2) \times 10^{14}$ cm^{-3} (appropriate for our samples) the mean nearest neighbour separation is about 120(95) nm. In absorption spectra from samples with this concentration we observe transitions for which the excited state has a radius less than this i.e. the $6p$ state, whose radial extent may be estimated to be $n^2 a_0 = 110$ nm. More precise effective mass calculations following Ref[19] produce $\sqrt{\langle r^2 \rangle} = 81$ nm. Excited states with a higher quantum number overlap with their neighbours, broadening the corresponding lines to the point where they are not observed in absorption spectroscopy. Stark broadening produced by random electric fields produced by ionized traps also affects the excited state, but can be eliminated by illumination with light just below the band edge (as we did here for our spectroscopy measurements). The isotopic composition primarily affects the ground state. The nearest neighbor (NN) Si isotope arrangement produces discrete states, which are clearest in the chalcogen donors[24,25],

where the total mass in the four NNs produces a significant shift in the energy. The isotopic randomness beyond the NN shell is responsible for the inhomogeneous broadening.

III. THEORY

It should be mentioned that different communities use different notations for different dynamical timescales such as the pure dephasing and inhomogeneous broadening times, and so we list some definitions for ease of reference. In the case of a neutral atomic system with discrete levels, excitation produces exponential relaxations of both the coherent polarisation

$$P(t) = P_0 \exp(-\frac{t}{T_2}) \tag{1}$$

in the rotating frame and the excited density

$$N(t) = N_0 \exp(-\frac{t}{T_1}) \tag{2}$$

with lifetimes T_2 and T_1 respectively. For a classical oscillator the polarization amplitude is proportional to the square root of the energy, and therefore decays half as fast. Similarly, in the case that the atoms are all identical, with no perturbations to atoms in the excited state other than the population relaxation out of it, then:

$$\frac{1}{T_2} = \frac{1}{2T_1}. \tag{3}$$

Additional perturbations that disturb the phase of the excited state but do not cause relaxation add to the dephasing rate

$$\frac{1}{T_2} = \frac{1}{2T_1} + \frac{1}{T_x} \tag{4}$$

where $1/T_x$ is the rate of loss of coherence due to the additional dephasing. In the case that the atoms are not all identical, then the decay of macroscopic coherences, i.e. free induction decay, occurs on a time scale that is shorter than T_1 or T_2, and we may write

$$\frac{1}{T_2^*} \sim \frac{1}{T_2} + \frac{1}{T_{\text{inhom}}} \tag{5}$$

where T_{inhom} is the timescale of the inhomogeneous phase loss, and T_2^* is the overall phase loss timescale. It should be mentioned that different communities use different notations for the different timescales, and since T_{inhom} is anyway not well-defined, neither is T_2^*. We shall make an explicit definition that applies to our case below.

In a time-domain, pump-probe experiment the transmission of the sample after an excitation pulse follows the same exponential decay as Eq. (2). For relaxation via intermediate states additional decay components can appear in the transmission. In the case of a short-lived metastable intermediate state the degenerate pump-probe transmission transient is unaffected, but for a long lived intermediate state the pump-probe shows one exponential component for the empying of the excited state and one for the refilling of the ground state. If the relaxation pathway involves ionization and recombination, then the associated transmission transient is a reciprocal decay not exponential.

The theory of frequency domain linewidths is just as complex. If the polarisation decays according to Eq. (1), i.e. a homogeneously broadened line for which the line centre is the same for all oscillators and the only perturbations that disturb the excitation are independent and identical for all oscillators, then the absorption spectrum can be obtained from the Fourier Transform of Eq. (1) and the resulting spectrum has Lorentzian shape. The Full-Width at Half Maximum (FWHM) of the Lorentzian in angular frequency is

$$\gamma = \frac{2}{T_2}. \tag{6}$$

When the line is inhomogeneously broadened we can find the spectrum if we know the probability distribution for the line-centres. If this distribution is a Gaussian then the overall lineshape that arises is the Voigt profile.

With the Voigt profile we may make a more precise statement about the contributions to the line width than that given in Eq. (5). Clearly, if γ and the FWHM in angular frequency of the Gaussian, β, are very different in magnitude, then the FWHM of the Voigt profile, which we call α, tends towards the larger of the two. A suitable approximate analytic expression for α is thus

$$\alpha = (1 - x)\gamma + (\beta^n + (x\gamma)^n)^{1/n} \tag{7}$$

where x and n are dimensionless parameters. If we define

$$\alpha = \frac{2}{T_2^*} \text{ and } \beta = \frac{2}{T_{\text{inhom}}} \tag{8}$$

then we recover Eq. (5) for $n = 1$. A much better fit[26] to the Voigt FWHM is obtained with $n = 2$ and $x = 0.4654$, for which the maximum inaccuracy is 0.02 %. Thus

$$\frac{1}{T_2^*} = \frac{0.5346}{T_2} + \sqrt{\frac{1}{T_{\text{inhom}}^2} + \frac{0.2166}{T_2^2}} \tag{9}$$

A fit of the Voigt profile allows extraction of γ, but the fit becomes less well constrained as γ/β becomes small.

IV. SAMPLES

The samples were produced at IKZ in Berlin[27]. Samples studied were single crystal silicon doped with bismuth, grown with the float zone (pedestal) technique, in the $\langle 100 \rangle$ orientation. Samples were cut from the same rod to 1 mm thickness with the surfaces chemically and mechanically polished with a 0.5° wedge to reduce interference effects from multiple reflections. One piece was doped with 1×10^{14} cm^{-3} Bi atoms and used for the absorption measurements, the other with 2×10^{14} cm^{-3} Bi atoms was used for the time domain measurements. As mentioned earlier concentration broadening is not expected to be different between the two samples, and the samples were of similar quality in all other respects.

Samples were of high crystal quality, with absorption and luminescence showing a low defect density. Both had a residual phosphorus doping, at least an order of magnitude lower concentration than the Bi donor.

In both frequency domain and time-domain experiments the samples were housed in a Janis super-vari-temp cryostat, with polymer windows, either immersed in superfluid He at 1.6 K, or cooled by flowing He vapour for measurements above 4.2 K. Sample temperature was monitored using a calibrated diode temperature sensor. For the time resolved experiments, the cryostat had HDPE windows on the outer vacuum chamber and cold polypropylene windows on the sample chamber. For the FTIR measurements both sets of windows were polypropylene. The samples were held strain free in a pouch. For the time resolved experiments, this was made using a piece of PCB and copper foil. Illumination of the sample was through a hole in the PCB.

V. TIME-DOMAIN PUMP-PROBE SPECTROSCOPY

The relaxation lifetimes of the excited states were measured via a balanced version of the pump-probe experiment, where a third pulse was used as a reference to balance out shot-to-shot noise and drift, see inset to Fig. 2. A strong pump pulse resonant in energy with the

transition of interest bleaches the absorption of the subsequent weak probe pulse, inducing maximum transmission. As time between the two pulses increases and more carriers relax back to the ground state, the absorption recovers. Since the probe absorption is proportional to the population difference between the ground and excited states the recovery time of the absorption is T_1.

Light was provided by the Dutch free electron laser FELIX, as intense, bandwidth limited pulses in the THz region of interest. The light arrived in macro-pulses of ~ 8 μs length at 10 Hz repetition rate, each containing a train of micro-pulses of ps duration at 25 MHz repetition rate. The spectral bandwidth was set to about 0.3% r.m.s., giving a Gaussian temporal profile of order 4 ps duration.

Each laser pulse was split into a pump pulse and a probe pulse using a pellicle beam splitter. The probe was then split into two identical pulses, one of which acted as a reference. The reference pulse was time delayed by 20 ns and placed co-linear with the probe at the same beamsplitter using a telescope arrangement which compensated for any transverse jitter of the probe. The probe and reference then followed the same path, through the sample and onto a liquid nitrogen cooled HgCdTe detector. The time delay between the pump and probe was set by varying the path length of the pump using a mechanical translation stage. Both beams were incident on the sample, separated by an angle of about 20°. To reduce the effect of scattered pump light on the detector the polarisation of the pump was set orthogonal to the probe and an analyser was placed in front of the detector. The intensity of the pulses was adjusted using wire grid attenuators. The beam spot on the sample had a diameter of about 1 mm. The probe and reference were measured using the same detector, by biasing the detector at 25 MHz, with the probe arriving during the positive bias and the reference during the negative bias using a phase locked amplifier circuit. A zero response of the circuit was produced when the probe and reference were in a balanced state. Any change in the absorption due to the pump pulse unbalanced the detector and a response was measured.

The signal was recorded using a National Instruments PXIE-5162 oscilloscope, with a digital boxcar average across the macro-pulse. Each time dependent pump-probe experiment was measured 3 times and averaged.

Experimental pump-probe results for the $2p_\pm$, $3p_\pm$ and $4p_\pm$ are shown in Fig. 2, with the extracted T_1 times quoted in the figure. These time domain measurements were performed at 1.6 K in superfluid He. The measured lifetimes were obtained from an exponential fit to

the decay curve, with an equation of the form:

$$S(t) = C + \frac{1}{2}(1 + \mathrm{erf}((t - t_0)/t_R))[Ae^{-(t-t_0)/T_1} + D] \tag{10}$$

where the factor involving the error function with time constant t_R represents the smooth population rise during the pump pulse, convolved with the probe pulse. At $t = -\infty$ the balancing technique should ensure that $S = 0$ and C should therefore be very close to 0, as observed in Fig. 2. The time at which the pump arrives, t_0, is arbitrary, but fixed to be the same for all experiments. The jump in transmission produced by the pump is A and T_1 is the lifetime of the upper state. The parameter D is related to the long lived population in intermediate or higher excited states or ionisation. The functional form of Eq. (10) is only appropriate for a single exponential decay, and is not appropriate for the case where there is an initially fast relaxation to an intermediate state followed by a slower decay back to the ground state discussed in the introduction, but no double exponential decays are visible in the raw data. We expect and generally find that $D \sim 0$ for the low lying states at low temperature and low illumination density, and D increases for higher lying states, temperatures and laser energy density in line with increased ionisation probability. The orbital level trend in D is seen in Fig. 2.

Errors were found from bootstrapping. In this process, statistically large numbers of artificial datasets of the same size were produced by randomly selecting points from the original dataset (with replacement, i.e. the same point may appear multiple times). Each artificial dataset was fitted in the same way using the best fit parameters as the starting point. The artificial dataset fit can sometimes fall into a local minimum, and those producing large Euclidian distance from the starting values were pruned. The standard deviation in a given fit parameter of the remaining bootstrap sets was used as its error. The resulting values of T_1 are shown in Fig. 2.

Finally we note that at high FELIX intensity where multi-photon processes might be important, the transients look different, and a long tail appears. The pump intensity was varied, over a range of attenuation from 0 to 10 dB. The data of Fig.. 2 were taken at the higher end of the intensity dependence (0, 0 and 5 dB for Fig. 2 a, b and c respectively), where the tail is just starting to appear. All of the T_1 values from lower intensity experiments down to 10 dB lie within the confidence intervals stated on Fig. 2.

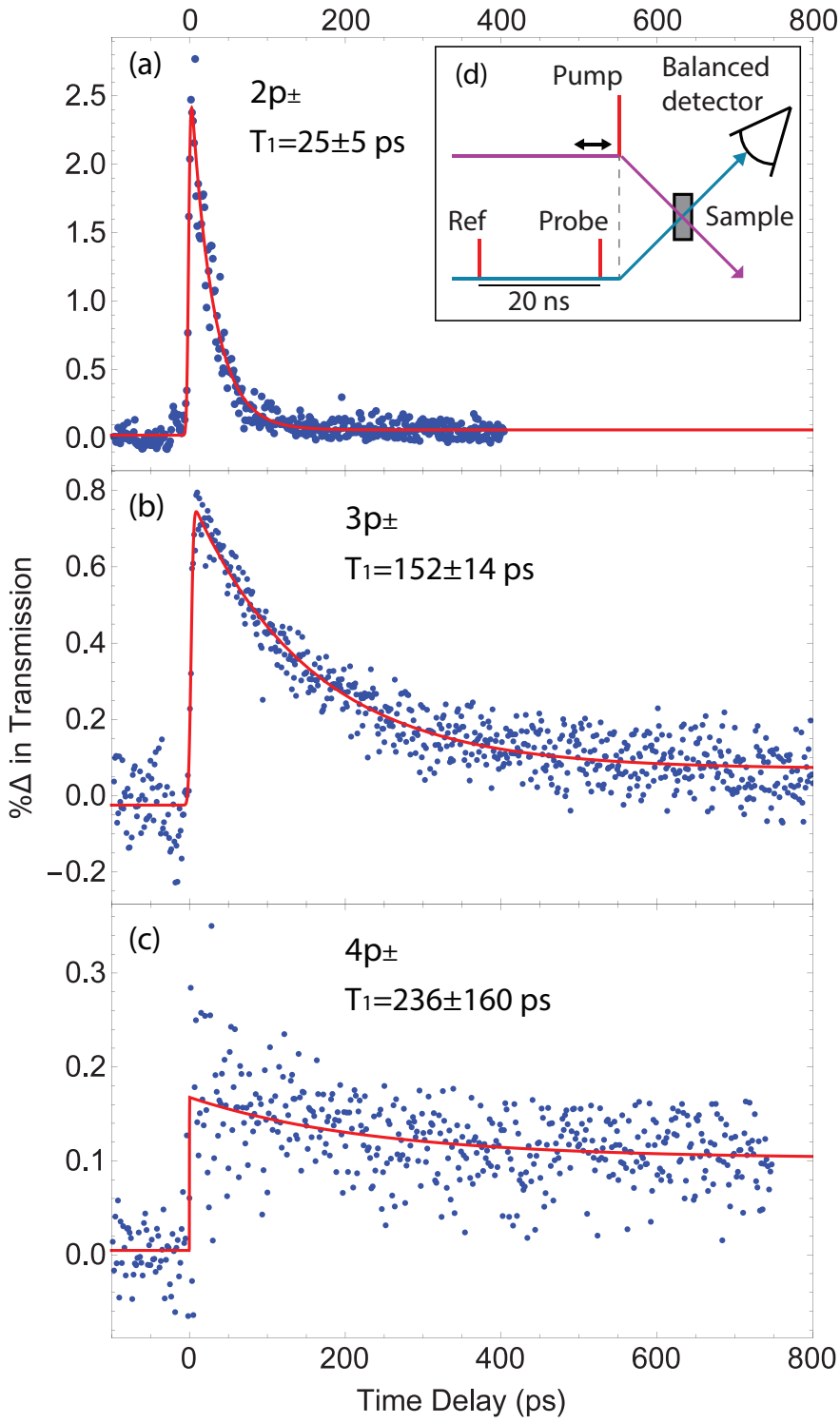

FIG. 2: Pump-probe data measured from the (a) $2p_{\pm}$, (b) $3p_{\pm}$, and (c) $4p_{\pm}$ transitions of the 2×10^{14} cm^{-3} Si:Bi sample, measured at 1.6 K with pump energy of 400 nJ, 360 nJ and 100 nJ per micro-pulse respectively. The laser bandwidth used was 0.3% of the central frequency. The red line is the fit to the data using Eq. (10), with the extracted lifetimes shown in the plot.

VI. FREQUENCY DOMAIN FTIR SPECTROSCOPY

The transmission spectrum was produced with a Bomem DA 8 FTIR with a resolution of 0.02 cm^{-1} (6×10^{-4} THz) and previously reported in Ref.[13]. The transmission was ratioed with a background spectrum, to find the absorbance $A = -\log_{10}(I/I_B)$. The results for transitions $1s(A) \rightarrow 2p_{\pm}$ to $1s(A) \rightarrow 6p_{\pm}$ are shown in Fig. 3.

It is clear that, apart from the broadening, each line in Fig 3 has the same structure, which is therefore all due to effects on the common ground state. The principal doublet structure is due to the hyper-fine interaction which produces two states with the electron spin either aligned or anti-aligned with the nuclear spin, with total spin either $F = 4$ or $F = 5$ and splitting with frequency Δ_{hf}. The hyperfine interaction is negligible in the odd parity excited states, which have a node at their centre. At Lq He temperature all ground state sublevels are equally populated, and total occupation probability is given simply by the multiplicity. The ratio of the areas under the lines is therefore expected to be $1:b = 11:9$, because the nuclear spin, $I_N = 9/2$, and this is very close to observation.

There is also a clear secondary doublet shifted to slightly lower frequency. Again, the same secondary doublet structure is observed in each line, so it must also be an effect in the ground state. We identify it with the arrangement of nearest neighbour silicon isotopes. This effect has previously been observed with the deeper S and Se impurity levels in silicon[24]. Heavier isotopes have smaller zero-point fluctuations, and this leads to a correction to the shape of the local crystal potential[28]. Since the four nearest neighbours are most important in determining the central cell correction[29], contributing half of the binding energy, it is the isotope arrangement of these atoms that is most influential. All the non-nearest host atoms contribute an average effective mass and the precise isotope arrangement is unimportant. The central cell correction has little effect on the excited states. As the measurements were made in ^{nat}Si which has 92.2 % ^{28}Si (with the rest ^{29,30}Si) we expect a probability of all 4 neighbours being ^{28}Si to be $P = 72$ %. The secondary doublet arises from the other less likely combinations. The ratio of the areas under the primary and secondary doublets, c, is thus expected to be $c = (1 - P)/P = 0.4$, which is very close to observation. As there is a range of the less likely combinations in the secondary doublet, it has thus broader inhomogeneous line-width than the primary doublet, but there is no reason to expect a different homogeneous contribution to the linewidth.

Upper state	$2p_\pm$	$3p_0$	$4p_0$	$3p_\pm$	$5p_0$	$4p_\pm$	$4f_0$	$5p_\pm$	$6p_\pm$
Frequency (THz)	15.617	15.836	16.361	16.409	16.619	16.633	16.704	16.809	16.900
Absorption ($\times 10^{-4}$)	5.65	0.48	0.17	1.47	0.18	0.46	0.15	0.39	0.13

TABLE I: Line centre of the lower frequency component of the principal hyperfine split doublet (orange curves in Fig. 3). Note these values are in units of frequency, $\nu = \omega/2\pi$. The dimensionless quantity proportional to the absorption $a_n(1 + b + c + bc)/\omega_n$ measured for each state.

The model described above for the origin of the lines leads to the following line-shape function, which we used to perform a fit of the measured absorbance of the n'th line:

$$A_n(\omega) = a_n \left[V(\omega; \omega_n, \gamma_n, \beta^{(p)}) + bV(\omega; \omega_n + \Delta_{hf}, \gamma_n, \beta^{(p)}) + cV(\omega; \omega_n + \delta, \gamma_n, \beta^{(s)}) + bcV(\omega; \omega_n + \delta + \Delta_{hf}, \gamma_n, \beta^{(s)}) \right] \tag{11}$$

where $V(\omega; \omega_0, \gamma, \beta)$ is the Voigt profile at angular frequency ω with line centre ω_0 and FWHMs γ and β for the Lorentzian and Gaussian parts respectively.

In this lineshape function we have assumed: that the homogeneous linewidth (γ) is the same for all four components; that the inhomogeneous linewidth is different for principal and secondary doublets ($\beta^{(p)}$ and $\beta^{(s)}$ respectively); that the principal and secondary doublets have the same hyperfine splitting (Δ_{hf}); and that the line strengths in the secondary doublet are in the same ratio ($b = 9/11$) as the principal doublet. Furthermore, we assumed that $\beta^{(p)}, \beta^{(s)}, \Delta_{hf}, \delta$ and c are independent of the state n (five global parameters), which leaves ω_n, γ_n and a_n as the three transition-dependent parameters. We discuss the effect of relaxing the assumptions at the end of this section.

The hyperfine splitting from this data is $\Delta_{hf} = 7.33 \pm 0.04$ GHz. The value is in good agreement with electron spin resonance measurements[7] of the hyperfine constant 1.4754 GHz, leading to an expected splitting $\Delta_{hf} = (I_N + 1/2)1.4754 = 7.377$ GHz. The frequency ω_n, i.e. the line centre of the lower frequency component of the principal doublet is shown in Table I.

The normalisation implies that $\int_{-\infty}^{\infty} \mathrm{d}\omega A_n(\omega) = a_n(1 + b + c + bc)$ so a_n has units of absorbance times angular frequency. Therefore $a_n(1 + b + c + bc)/\omega_n$ is a dimensionless measure of the absorption that is independent of the broadening, and simply proportional to the cross-section, the oscillator strength and the square of the dipole moment. This value for each state is quoted in Table I.

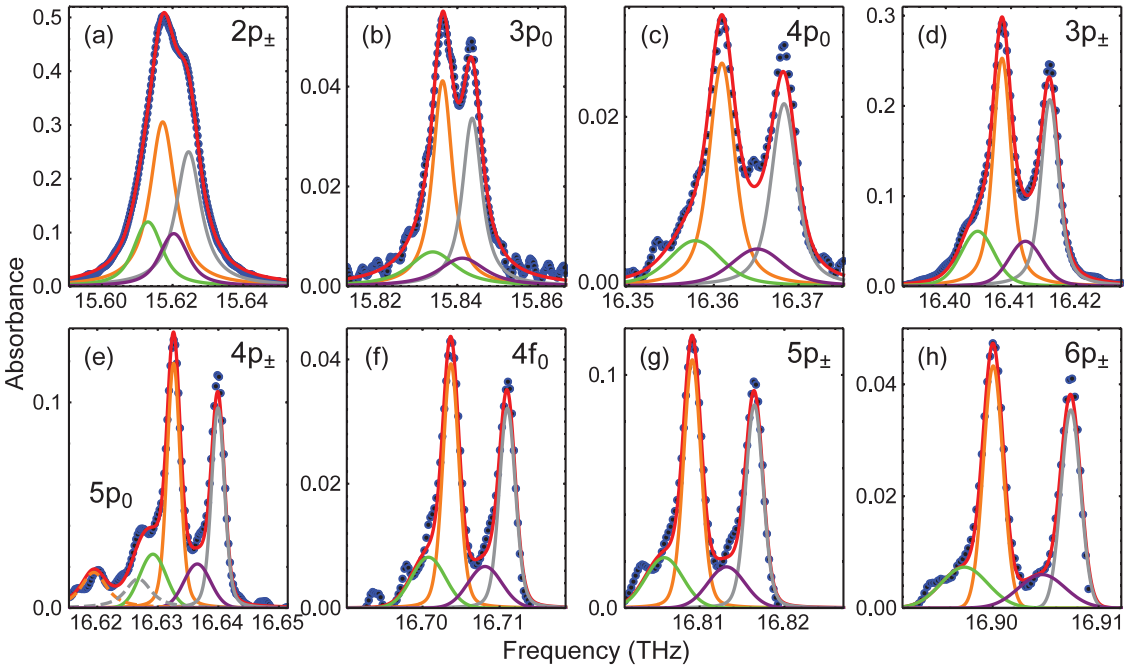

FIG. 3: Fits to the FTIR data. From the top left the lines are: $2p_\pm$, $3p_0$, $4p_0$, $3p_\pm$, $5p_0/4p_\pm$, $4f_0$, $5p_\pm$, and $6p_\pm$. See text for details of the fitting. The experimental absorbance vs. frequency is shown with the blue points and the combined Voigt fit with the red lines. The orange and grey lines are the principle, and the purple and green lines, the secondary components to the total fit. The dashed lines are used to separate the $5p_0$ from the $4p_\pm$. FTIR data from Ref.[13].

The values of $T_{2n} = 2/\gamma_n$ from the fits are given in Fig. 4, along with the values of $T^*_{2n} = 2/\alpha_n$, the inverse of the FWHM of $V(\omega;\omega_n,\gamma_n,\beta)$ for the principal doublet.

We tried a completely unrestricted fit, i.e. $\gamma_n^{(p)}$ and $\gamma_n^{(s)}$ different for principal and secondary doublets, and all parameters including $\beta_n^{(p)}, \beta_n^{(s)}$ etc were allowed to vary with n. We did not obtain any interesting difference in the fit values for the important quantities ω_n, γ_n and a_n, but the bootstrap errors for every transition were at least an order of magnitude larger (due to correlations between the fit parameters), and these are the errors shown on Fig. 4, since they represent the systematic errors produced by the assumptions in Eq. (11).

VII. DISCUSSION

Values of $2T_1$ from the pump-probe decay are shown on Fig. 4 for comparison with the values of T_2 derived from the absorption spectra, showing a broad agreement within

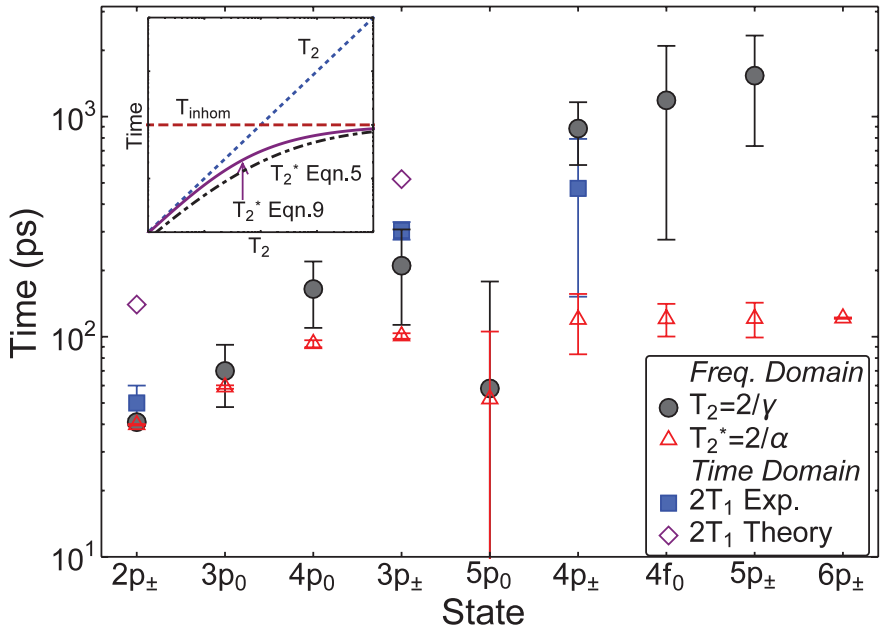

FIG. 4: Comparison of time-domain and frequency domain results. (Black circle) $T_2 = 2/\gamma$ ps from fits to the absorption spectra described in the text, (red triangle) the $T_2^* = 2/\alpha$ from Eq. (9) using data from the fits to the absorption spectrum, (blue square) $2T_1$ from the pump-probe measurements, and (purple diamond) $2T_1$ from the theory of Ref.[22]. The T_2 value for the $6p_\pm$ is off the scale, and this line may be considered completely inhomogeneously broadened. Inset: a Log-Log plot showing a comparison between the T_2^* as a function of T_2 calculated either exactly, or approximately using Eq. (5) or Eq. (9), with a constant T_{inhom}. The results from Eq. (9) and the exact inverse FWHM of the Voigt profile are indistinguishable on the scale shown in the figure.

experimental error. It is clear that $T_2 = 2/\gamma$ for the $2p_\pm$ state absorption agrees very well with $2T_1$ from the pump probe, leading to negligible extra dephasing ($1/T_x \simeq 0$). The residual P concentration provides centres with an lower binding energy than the laser photons used, and could therefore produce extra conduction electrons. Evidently they had no effect on the dephasing. For the $3p_\pm$ and $3p_0$ states, the agreement is also good, although the uncertainty in $2/\gamma$ is much higher due to the difficulty in extracting γ from the Voigt profile when $\gamma < \beta$ (and the same is true for the other excited states on Fig. 4). The uncertainty in T_1 is also higher in these cases due to the weaker transitions. The FWHM of each line, α, is much better determined, and its inverse, T_2^*, is systematically shorter than the $2T_1$ or T_2 value discussed above, and, for the higher lying states, independent of the state because of our assumption of fixed β. The small error in T_2^*, found when this assumption was relaxed,

justifies the state independent β.

As measured above, the $1s-2p_0$ transition shows a very broad line, because the energy matches that of the optical phonons, producing a very fast decay rate, and we were not able to obtain a pump-probe signal from this transition. The $1s-2p_\pm$ transition is probably also influenced by its close proximity in energy to these optical phonons, producing a shorter lifetime than the same transition in other donor species.

The lifetimes for $2p_\pm$ and $3p_\pm$ seem broadly consistent with the calculated intra-valley relaxation to the $2p_0$ state[22] (Fig. 4 diamonds), indicating that they are likely to be responsible for the first step in a two-step cascade, followed by TO phonon emission to the ground state.

More pump-probe data on other lines would also be useful however as shown in Fig. 3 are either significantly weaker or close together. The experiment of Fig 2 c on the $4p_\pm$ was at our sensitivity limit, and Fig. 3 e shows the absorbance to be 0.1 in that case. The next strongest line, $5p_\pm$ has similar absorbance but is spaced less than 0.1 THz from adjacent lines. The bandwidth limited pulses from FELIX have a width of 50 GHz r.m.s. making it difficult to separate contributions from the adjacent excited states. For higher doped samples, which would give a stronger absorption, the higher lying wavefunctions overlap, and for thicker samples beam overlap becomes a problem.

VIII. CONCLUSION

In summary, the FTIR and pump-probe data are complementary. We have shown that in the case of Si:Bi, the low energy transitions are mainly homogeneously broadened, and that there is little, if any extra dephasing, i.e. $T_2 = 2T_1$. For the higher lying lines the homogeneous broadening becomes unimportant relative to the inhomogeneous broadening, i.e. the Lorentzian component in the spectrum is obscured. Isotopically pure ^{28}Si doped with Bi would be very interesting from this point of view. In the absence of such samples, it is very difficult to unambiguously obtain T_2 for those high-lying lines. For some transitions the pump-probe technique is able to obtain T_1 in this situation, though it also becomes more and more difficult as the high-lying lines become weaker and closer together. A two step cascade via the $2p_0$ state seems the most likely relaxation process for the excited orbital states of Si:Bi.

Acknowledgments

We gratefully acknowledge the Stichting voor Fundamenteel Onderzoek der Materie (FOM) for the support of the FELIX Laboratory and the financial support from the UK Engineering and Physical Sciences Research Council [COMPASSS/ADDRFSS, Grant No. EP/M009564/1]. B.N.M. is grateful for a Royal Society Wolfson Research Merit Award. The spectroscopic work at SFU was supported by the Natural Sciences and Engineering Research Council of Canada.

---

* Electronic address: b.murdin@surrey.ac.uk

[1] B. E. Kane, Nature **393**, 133 (1998).

[2] F. A. Zwanenburg, A. S. Dzurak, A. Morello, M. Y. Simmons, L. C. L. Hollenberg, G. Klimeck, S. Rogge, S. N. Coppersmith, and M. A. Eriksson, Reviews of Modern Physics **85**, 961 (2013).

[3] A. Morello, J. J. Pla, F. A. Zwanenburg, K. W. Chan, K. Y. Tan, H. Huebl, M. Möttönen, C. D. Nugroho, C. Yang, J. A. van Donkelaar, et al., Nature **467**, 687 (2010).

[4] M. Steger, K. Saeedi, M. L. W. Thewalt, J. J. L. Morton, H. Riemann, N. V. Abrosimov, P. Becker, and H.-J. Pohl, Science **336**, 1280 (2012).

[5] K. Saeedi, S. Simmons, J. Z. Salvail, P. Dluhy, H. Riemann, N. V. Abrosimov, P. Becker, H.-J. Pohl, J. J. L. Morton, and M. L. W. Thewalt, Science **342**, 830 (2013).

[6] G. Wolfowicz, A. M. Tyryshkin, R. E. George, H. Riemann, N. V. Abrosimov, P. Becker, H.-J. Pohl, M. L. W. Thewalt, S. A. Lyon, and J. J. L. Morton, Nature Nanotechnology **8**, 561 (2013).

[7] G. W. Morley, M. Warner, A. M. Stoneham, P. T. Greenland, J. Van Tol, C. W. M. Kay, and G. Aeppli, Nature Materials **9**, 725 (2010).

[8] A. M. Stoneham, A. J. Fisher, and P. T. Greenland, Journal of Physics: Condensed Matter **15**, L447 (2003), URL http://stacks.iop.org/0953-8984/15/i=27/a=102.

[9] N. Q. Vinh, P. T. Greenland, K. Litvinenko, B. Redlich, A. F. G. Van Der Meer, S. A. Lynch, M. Warner, A. M. Stoneham, G. Aeppli, D. J. Paul, et al., Proceedings of the National Academy of Sciences **105**, 10649 (2008).

[10] K. L. Litvinenko, P. T. Greenland, B. Redlich, C. R. Pidgeon, G. Aeppli, and B. N. Murdin, Phys. Rev. B **94**, 235207 (2016), URL http://link.aps.org/doi/10.1103/PhysRevB.94.

235207.

[11] P. T. Greenland, S. A. Lynch, A. F. G. van der Meer, B. N. Murdin, C. R. Pidgeon, B. Redlich, N. Q. Vinh, and G. Aeppli, Nature **465**, 1057 (2010), URL http://dx.doi.org/10.1038/nature09112.

[12] K. L. Litvinenko, E. T. Bowyer, P. T. Greenland, N. Stavrias, J. Li, R. Gwilliam, B. J. Villis, G. Matmon, M. L. Y. Pang, B. Redlich, et al., Nature Communications **6**, 6549 (2015).

[13] K. Saeedi, M. Szech, P. Dluhy, J. Z. Salvail, K. J. Morse, H. Riemann, N. V. Abrosimov, N. Nötzel, K. L. Litvinenko, B. N. Murdin, et al., Scientific Reports **5**, 10493 (2015).

[14] B. Pajot, J. Kauppinen, and R. Anttila, Solid State Communications **31**, 759 (1979), ISSN 0038-1098, URL http://www.sciencedirect.com/science/article/pii/0038109879907841.

[15] N. R. Butler, P. Fisher, and A. K. Ramdas, Phys. Rev. B **12**, 3200 (1975), URL http://link.aps.org/doi/10.1103/PhysRevB.12.3200.

[16] A. K. Ramdas and S. Rodriguez, Reports on Progress in Physics **44**, 1297 (1981), URL http://stacks.iop.org/0034-4885/44/i=12/a=002.

[17] B. Pajot, *Optical absorption of impurities and defects in semiconducting crystals i. Hydrogen-like Centers*, Springer series in solid-state sciences 158 (Springer, 2010).

[18] M. Steger, A. Yang, D. Karaiskaj, M. L. W. Thewalt, E. E. Haller, J. W. Ager, M. Cardona, H. Riemann, N. V. Abrosimov, A. V. Gusev, et al., Phys. Rev. B **79**, 205210 (2009), URL https://link.aps.org/doi/10.1103/PhysRevB.79.205210.

[19] B. N. Murdin, J. Li, M. L. Y. Pang, E. T. Bowyer, K. L. Litvinenko, S. K. Clowes, H. Engelkamp, C. R. Pidgeon, I. Galbraith, N. V. Abrosimov, et al., Nature Communications **4**, 1469 (2013).

[20] A. J. Mayur, M. D. Sciacca, A. K. Ramdas, and S. Rodriguez, Phys. Rev. B **48**, 10893 (1993), URL https://link.aps.org/doi/10.1103/PhysRevB.48.10893.

[21] C. Flensburg and R. F. Stewart, Phys. Rev. B **60**, 284 (1999), URL https://link.aps.org/doi/10.1103/PhysRevB.60.284.

[22] V. V. Tsyplenkov, R. K. Zhukavin, and V. N. Shastin, Semiconductors **48**, 1017 (2014), ISSN 1090-6479, URL http://dx.doi.org/10.1134/S1063782614080247.

[23] S. G. Pavlov, H.-W. Hübers, M. H. Rümmeli, R. K. Zhukavin, E. E. Orlova, V. N. Shastin, and H. Riemann, Applied Physics Letters **80**, 4717 (2002), URL http://scitation.aip.org/content/aip/journal/apl/80/25/10.1063/1.1489080.

[24] M. Steger, A. Yang, M. L. W. Thewalt, M. Cardona, H. Riemann, N. V. Abrosimov, M. F.

Churbanov, A. V. Gusev, A. D. Bulanov, I. D. Kovalev, et al., Phys. Rev. B **80**, 115204 (2009), URL https://link.aps.org/doi/10.1103/PhysRevB.80.115204.

[25] B. Pajot, B. Clerjaud, and M. D. McCluskey, Phys. Rev. B **69**, 085210 (2004), URL https://link.aps.org/doi/10.1103/PhysRevB.69.085210.

[26] J. J. Olivero and R. L. Longbothum, Journal of Quantitative Spectroscopy and Radiative Transfer **17**, 233 (1977).

[27] H. Riemann, N. Abrosimov, and N. Nötzel, ECS Transactions **3**, 53 (2006).

[28] M. Cardona and M. L. W. Thewalt, Rev. Mod. Phys. **77**, 1173 (2005), URL https://link.aps.org/doi/10.1103/RevModPhys.77.1173.

[29] J. K. Gamble, N. T. Jacobson, E. Nielsen, A. D. Baczewski, J. E. Moussa, I. Montaño, and R. P. Muller, Phys. Rev. B **91**, 235318 (2015), URL https://link.aps.org/doi/10.1103/PhysRevB.91.235318.